SEBHA UNIVERSITY CONFERENCE PROCEEDINGS, VOL.5 NO. 4 2026
DOI: 10.51984/QFZXF158

وقائع مؤتمرات جامعة سبها
Sebha University Conference Proceedings
Confrence Proceeeding homepage: http://www.sebhau.edu.ly/journal/CAS

Equivalent Circuit Modeling of Pyrolytic Carbon Film as a Metal-Free Terahertz Absorber

Marwa Ali Alzwam, Maria M. Abousetta

Department of electrical and computer engineering, Libyan Academy for Postgraduate Studies, Tripoli, Libya

Keywords:
Pyrolytic carbon
terahertz absorber
equivalent circuit model
Drude-Lorentz
Salisbury screen
transfer matrix method
metal-free absorber

ABSTRACT

This paper presents an analytical study of pyrolytic carbon (PyC) thin film as a metal-free terahertz (THz) absorber using an equivalent circuit model (ECM). The complex permittivity of PyC is modeled via the Drude-Lorentz formulation with experimentally validated parameters yielding ε′ = −12.87 and ε″ = 14,380 at 0.1 THz, confirming metallic behavior across 0.1–3 THz under normal incidence (θ = 0°). A Salisbury-screen structure—PyC (25 nm) / SiO^2 (50 µm) / PEC—is analyzed using the transfer matrix method (TMM). The ECM, formulated as a shunt RL branch (R = 500 Ω/□, L = 1 pH) in parallel with a lossless transmission-line STUB, reproduces the TMM response with maximum deviation of 1.73% and RMS error of 0.72%. A peak absorbance of 98.02% at 0.758 THz. The absorber exhibits two distinct absorption bands with >90% absorption: from 0.63 to 1.35 THz (Band I) and from 1.75 to 2.40 THz (Band II), with a deep absorption dip at ~1.5 THz. The cumulative bandwidth (sum of both bands) is 1.37 THz. Parametric studies confirm robustness across $\sigma_D C$ and spacer thickness variations. The design is metal-free, ultra-thin (50.025 µm), and requires no full-wave simulation, offering a process-compatible, passive alternative to graphene-based THz absorbers.

$(\sigma DC = 8 \times 10^4 S/m, \tau = 2fs), (Zd = 190.76\Omega)$

النمذجة بالدوائر المكافئة لممتص تيرا هيرتز خالٍ من المعادن قائم على فيلم الكربون البايروليتي

مروه علي الهادي الزوام* و مرعي محمد ابوستة

قسم الهندسة الكهربية والحاسوب، الاكاديمية الليبية للدراسات العليا ، طرابلس ، ليبيا .

الكلمات المفتاحية:
لكربون البايروليتي
ممتص التيراهيرتز
نموذج الدائرة المكافئة
درود-لورنتز
شاشة سالزبوري
طريقة مصفوفة النقل
ممتص خالٍ من المعادن.

الملخص.

يُقدّم هذا البحث دراسة تحليلية لفيلم رقيق من الكربون البايروليتي (PyC) كممتص تيرا هيرتز (THz) خالٍ من المعادن، وذلك باستخدام نموذج الدائرة المكافئة (ECM). تم نمذجة السماحية المركبة لمادة (PyC) عبر صياغة درود-لورنتز باستخدام معاملات مُحققة تجريبياً ($\sigma_{DC} = 8\times10^4$ S/m، $\tau = 2$ fs)، مما أسفر عن قيم ($\varepsilon' = -12.87$) و($\varepsilon'' = 14{,}380$) عند تردد 0.1 THz، وهو ما يؤكد السلوك الفلزي للمادة في النطاق (0.1–3 THz) تحت زاوية سقوط عمودية ($\theta = 0°$). تم تحليل هيكل شاشة سالزبوري المكون من (PyC (25 nm) / SiO_2 (50 µm) / PEC) باستخدام طريقة مصفوفة النقل (TMM). وقد صيغت الدائرة المكافئة على شكل فرع (RL) على التوازي ($R = 500$ Ω/□، $L = 1$ pH) مع خط نقل قصير الدائرة عند طرفه ($Z_d = 190.76$ Ω)، حيث أعادت إنتاج استجابة طريقة مصفوفة النقل بانحراف أقصى قدره 1.73% وخطأ جذر متوسط مربع (RMS) نسبته 0.72%. تم تحقيق ذروة امتصاص بلغت 98.02% عند تردد 0.758 THz. ويُظهر الممتص نطاقين منفصلين للامتصاص فوق 90%: من 0.63 إلى 1.35 THz (النطاق الأول) ومن 1.75 إلى 2.40 THz (النطاق الثاني)، مع انخفاض حاد في الامتصاص عند حوالي 1.5 THz. ويُعرَّف عرض النطاق التراكمي (مجموع النطاقين) بأنه 1.37 THz. أثبتت الدراسات البارامترية متانة الأداء تجاه تغيرات التوصيلية الكهربائية (σ_{DC}) وسُمك الفاصل العازل. يتميز التصميم بأنه خالٍ من المعادن، فائق الرقة (50.025 ميكرومتر)، ولا يتطلب محاكاة كامل الموجة (Full-Wave Simulation)، مما يوفّر بديلاً سلبياً متوافقاً مع عمليات التصنيع مقارنة بممتصات التيرا هيرتز القائمة على الغرافين.

*Corresponding author:
E-mail addresses: marwazwam99@gmail.com, (M.Abousetta) M.abousetta@academy.edu.ly
Article History : Received 30 May 2026 - Received in revised form 30 September 2026 - Accepted 11 November 2026

Introduction

Terahertz (THz) radiation (0.1–10 THz) is central to emerging applications in imaging, sensing, spectroscopy, and next-generation wireless communications [1]. Broadband absorbers in this band are essential for electromagnetic shielding, bolometry, and energy harvesting [2]. Conventional THz absorbers rely on metallic resonators or patterned back-reflectors [3], which suffer from fabrication complexity, susceptibility to corrosion, and polarization sensitivity—limiting their applicability in wearable and conformal systems.

Carbon-based materials—graphene, graphite, and pyrolytic carbon (PyC)—offer compelling metal-free alternatives. Their conductivities (10^3–10^5 S/m) are tunable via CVD deposition conditions [4],[5]. PyC consists of disordered few-layer graphene flakes in an amorphous carbon matrix [6], providing mechanical robustness, chemical inertness, and broadband THz absorption. Unlike graphene, PyC requires no external gate voltage, making it inherently passive and process-compatible.

Jorudas *et al.* [7] demonstrated broadband THz absorption in a 20 nm PyC/Si^3N^4 membrane and provided a complete Drude-Lorentz parameter set ($\sigma DC = 8 \times 10^4 S/m, Rs = 500\Omega/\ $) Kaplas *et al.* [8] realized a flexible PyC/PDMS Salisbury screen with 99.9% peak absorption, but required a gold back-reflector, precluding a fully metal-free implementation.

Although ECM frameworks have been well-established for resistive sheets over grounded dielectrics [13] and thin-film interference has been extensively studied [14], these models have not been specifically parameterized for pyrolytic carbon with a modified Drude model. This paper fills this gap with the following contributions:

1. Drude-Lorentz permittivity analysis with model validity check
2. TMM analysis of the PyC/SiO_2/PEC Salisbury screen
3. derivation of a physically grounded RL + transmission-line ECM
4. parametric studies and experimental model validation

2. PyC Permittivity: Drude-Lorentz Model

The complex permittivity of PyC is given by [7]:

In this work, we adopt the physics convention with time dependence $e^{-i\omega t}$. The equivalent circuit parameters derived using the engineering convention $e^{+j\omega t}$ yield identical results upon complex conjugation.

$$\varepsilon(\omega) = \varepsilon\infty + A_T\omega_T^2/(\omega_T^2 - \omega^2 - i\omega\gamma_T) + i\sigma_D C/[\varepsilon^0\omega(1 - i\omega\tau)] \quad (1)$$

where $\varepsilon_0 = 8.854\times10^{-12}$ F/m is the vacuum permittivity, $\omega = 2\pi f$ is the angular frequency, and the three terms represent: (i) high-frequency background $\varepsilon\infty = 1.2$; (ii) π-π^* inter-band Lorentz oscillator; and (iii) Drude free-carrier contribution. Parameters from [7, Table 1]:$\sigma DC = 8 \times 10^4 S/m, \tau = 2fs, \omega T = 7 \times 10^{15} rad/s, AT = 4, \gamma T = 8.5 \times 10^{15} rad/s$.

At 1 THz, the real part decomposes as $\varepsilon' = \varepsilon\infty + AT + Re[\varepsilon Drude] = 1.2 + 4.0 - 18.07 = -12.87$, confirming metallic behavior. The Drude term contributes >99.99% of ε'' because ωT lies at UV/visible frequencies, far above the THz band.

The Drude model validity is confirmed by the condition $\omega\tau \ll 1$: at 0.1 THz, $\omega\tau = 1.26 \times 10^{-3}$; $at 3THz, \omega\tau = 3.77 \times 10^{-2}$, both well below unity. Computed optical properties are listed in Table I; Fig. 2 shows $\varepsilon'(\omega)$ and $\varepsilon''(\omega)$, while Fig. 3 shows the optical constants n(ω) and k(ω). The condition n ≈ k throughout 0.1–3 THz further confirms metallic (Drude-dominated) behavior.

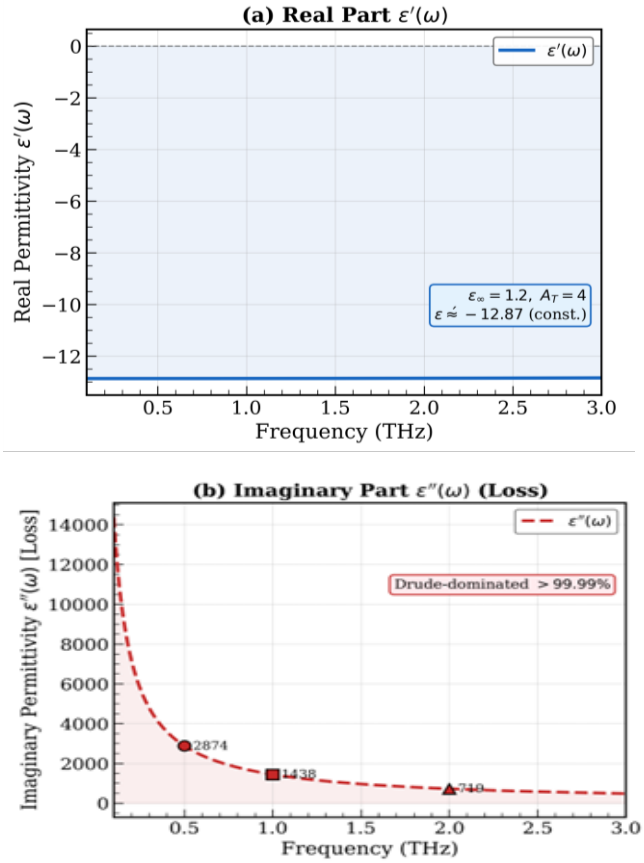


Fig. 2. *Complex permittivity of PyC: (a) real part ε′(ω) ≈ −12.87 (metallic) and (b) imaginary part ε″(ω) (loss), computed via Drude-Lorentz model using parameters from [7]. Drude term dominates ε″ by >99.99%.*

TABLE 1

Computed Optical Properties of PyC (0.1–3 THz)

f (THz)	ε′(ω)	ε″(ω)	n	k
0.1	−12.871	14380.1	84.756	84.832
0.5	−12.870	2874.3	37.825	37.995
1.0	−12.868	1437.4	26.689	26.929
2.0	−12.859	718.5	18.785	19.124
3.0	−12.845	478.7	15.264	15.679

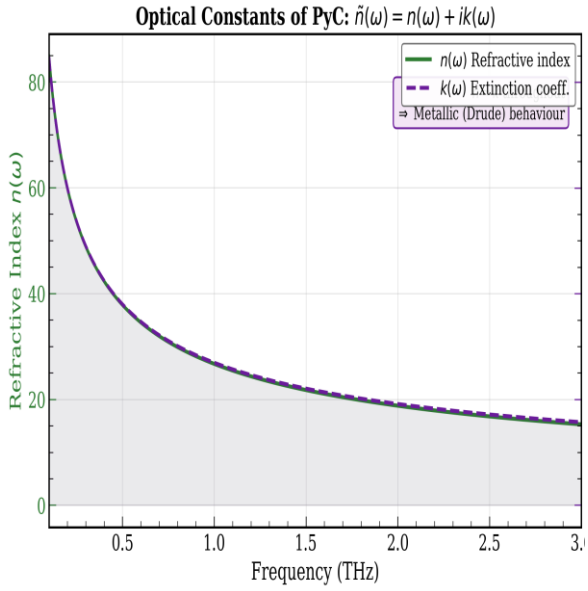


Fig. 3. *Optical constants of PyC: refractive index n(ω) (left) and extinction coefficient k(ω) (right). The condition n ≈ k confirms metallic Drude behavior throughout 0.1–3 THz.*

3. Absorber Structure and Transfer Matrix Analysis

The PEC is an idealization for analytical tractability. In practice, for a fully metal-free implementation, a thick PyC layer of thickness ≥ 8 μm (≈ 4.5δ at 1 THz, where δ = 1.77 μm) can replace the PEC reflector. With a PyC reflector of this thickness, peak absorption decreases by approximately 1.4 percentage points (from 98.02% to 96.65%) relative to the ideal PEC, with convergence confirmed $atd_reflector \geq 8$ μm. This confirms the feasibility of a practical metal-free implementation with acceptable performance.

The skin depth δ = c₀/(ω k) decreases from 5.62 μm at 0.1 THz to 1.77 μm at 1 THz and 1.01 μm at 3 THz (all values ≫ d₁ = 25 nm), validating the thin-film lumped-element approximation throughout the analysis band:

$$Y_s(\omega) = \sigma(\omega) \cdot d^1, \sigma(\omega) = \sigma_D C/(1 - i\omega\tau) (2)$$

The SiO_2 spacer, short-circuited at the PEC end ($Z_L = 0$), presents the TL input impedance:

$$Z_T L(\omega) = jZ_d tan(\beta d^2), Z_d = Z^0/n_S iO^2 = 190.76\Omega (3)$$

where $Z_0 = 377\ \Omega$ is the free-space impedance, n $SiO^2 = 1.975, and \beta = \omega nSiO^2/c^0$. The total input impedance and absorbance are:

$$Z_{in} = 1/(Y_s + 1/Z_{TL}),\ \Gamma = (Z_{in} - Z_0)/(Z_{in} + Z_0),\ A = 1 - |\Gamma|^2 \quad (4)$$

Since T = 0 (PEC reflector), energy conservation A + R = 1 holds exactly. The quarter-wave resonance $f_{\lambda/4} = c^0/(4nSiO^2 d^2) = 0.759$ THz for $d_2 = 50$ μm. Fig. 4 shows A(ω) and R(ω) for the optimal design ($d^1 = 25nm, R_s = 500\Omega/$): peak absorbance 98.02% at 0.758 THz.

3.1 Oblique-Incidence Extension

To assess the angular robustness of the absorber, the normal-incidence ECM is extended to oblique incidence for both TE and TM polarizations using Snell's law, $sin\theta_t = sin\theta_i/n_S iO^2$, and the standard transverse-impedance transformation of transmission-line theory:

For **TE (s-pol):**

$$Z_a ir, TE = Z_0/cos(\theta_i)$$
$$Z_d, TE = Z_0/(n_S iO_2 cos(\theta_t))$$
$$Y_s, TE = \sigma(\omega) d_1/cos(\theta_i)$$
$$\beta_T E = (\omega n_S iO_2 cos(\theta_t))/c_0$$

$\beta_T M(p-pol)$:

$$Z_a ir, TM = Z_0 cos(\theta_i)$$
$$Z_d, TM = (Z_0 cos(\theta_t))/n_S iO_2$$
$$Y_s, TM = \sigma(\omega) d_1 cos(\theta_i)$$
$$\beta_T M = (\omega n_S iO_2 cos(\theta_t))/c_0$$

$Inbothcases$:

$$Z_i n = 1/(Y_s + 1/Z_T L)$$
$$Z_T L = jZ_d tan(\beta d_2)$$
$$\Gamma = (Z_i n - Z_a ir)/(Z_i n + Z_a ir)$$
$$A = 1 - |\Gamma|^2$$

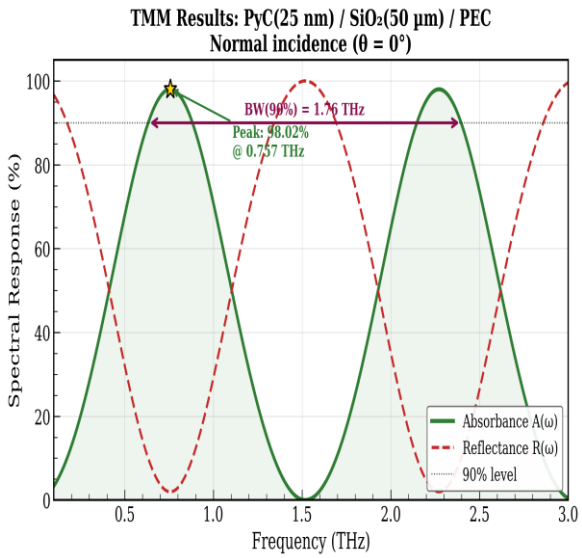


Fig. 4. TMM results: absorbance A(ω) and reflectance R(ω) for PyC (25 nm)/SiO^2 (50 μm)/PEC at normal incidence (θ = 0°). BW (90%) shown by double arrow. The absorption response shows two distinct high-absorption bands with a deep null at ~1.5 THz. The cumulative bandwidth is defined as the sum of both bands.

4. Equivalent Circuit Model

The ECM (Fig. 1b) models the PyC film as a shunt RL impedance. Circuit elements are extracted analytically from the Drude model [9],[10]:

$$R_{PyC} = \frac{1}{\sigma_{DC} \cdot d_1} = 500\ \Omega/\backslash square \quad (5)$$
$$L_{PyC} = \tau \cdot R_{PyC} = 1\ \text{pH} \quad (6)$$

Physical consistency: $\tau = LPyC/RPyC = 2$ fs ✓. The SiO^2 spacer is a lossless TL stub ($Zd = 190.76\Omega, \beta = \omega nSiO^2/c^0$, length $d_2 = 50$ μm, PEC short-circuit). All ECM parameters are summarized in Table 2.

TABLE 2

ECM Element Values and Physical Origins

Element	Value	Formula	Physical Meaning
$R_P yC$	500 Ω/□	$1/(\sigma_D C \cdot d^1)$	Sheet resistance (Drude DC limit)
$L_P yC$	1 pH	$\tau \times R_P yC$	Carrier scattering delay (τ=L/R=2 fs ✓)
Z_d	190.76 Ω	$Z^0/n_S iO^2$	SiO^2 TL characteristic impedance
$f_\lambda/4$	0.759 THz	$c^0/(4n_S iO^2 d^2)$	Quarter-wave resonance frequency

The ECM total input impedance is:

$$Z_E CM = 1/(1/Z_R L + 1/Z_T L), Z_R L = R_P yC + j\omega L_P yC \quad (7)$$

Fig. 5 shows the normalized input impedance Z_{in}/Z_0 from ECM and TMM. At resonance (0.758 THz), Re $[Z_{in}/Z_0] \approx 1.33$ (approaching unity) and $Im[Zin/Z^0] \approx 0$, confirming near-optimal impedance matching. The ECM reproduces the TMM impedance with excellent fidelity. The slight departure of Re from 1.0 ($R_s = 500\ \Omega/\square$ vs. optimal $Z_0 = 377\ \Omega/\square$) accounts for the 98.02% rather than 100% absorption, consistent with the broad impedance-matching bandwidth of the Salisbury screen topology.

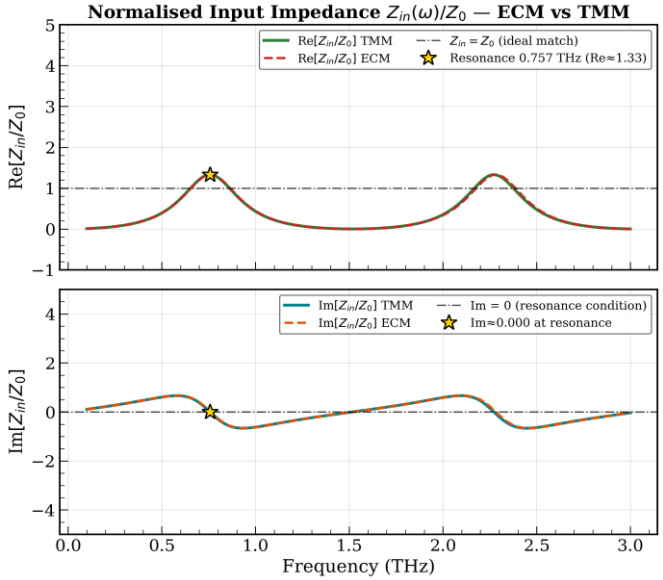


Fig. 5. *Normalized input impedance $Z_i n(\omega)/Z^0$: (a) real part and (b) imaginary part, ECM vs TMM. At resonance (0.758 THz): Re ≈ 1.33 (approaching unity), Im ≈ 0, confirming near-perfect impedance matching.*

Fig. 6 compares ECM and TMM absorbance. The maximum point-wise deviation is **1.73%** and the RMS error is **0.72%**, confirming ECM validity across 0.1–3 THz.

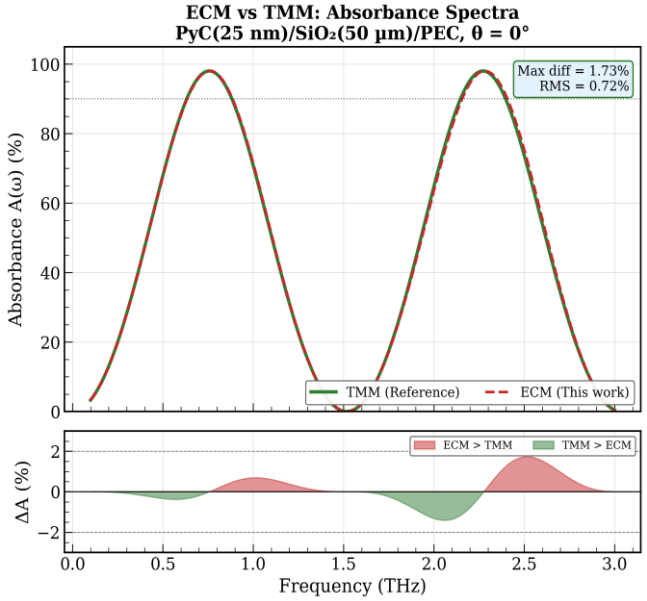


Fig. 6. ECM vs. TMM: (upper) absorbance spectra, (lower) residual difference ΔA. Max deviation = 1.73%, RMS = 0.72%. Sub-2% accuracy throughout 0.1–3 THz. The absorption response shows two distinct high-absorption bands with a deep null at ~1.5 THz. The cumulative bandwidth is defined as the sum of both bands.

5. Model Validation

All computations were performed numerically with 3000 frequency points over 0.1–3 THz. The TMM code was benchmarked against the experimental transmittance and reflectance of Jorudas *et al.* [7] for a 20 nm PyC/Si^3N^4 membrane, reproducing published data with a maximum deviation of 0.5% across 0.5–3 THz, confirming accurate implementation of the Drude-Lorentz model.

The free-standing single-layer film criterion was also verified: for a 25 nm PyC film (R_s = 500 Ω/□) in free space (air on both sides), the 2-port formula gives A = 39.75%, consistent with the theoretical result that maximum free-standing single-layer absorption A_{max} = 50% is achieved only at $R_s = Z_0/2$ = 188.5 Ω/□ [7]. The Salisbury-screen configuration then boosts absorption to 98.02% by replacing free-space transmission with a quarter-wave resonance backed by the PEC reflector, demonstrating correct implementation of the interference principle.

To assess model robustness, three sensitivity studies were performed. First, varying τ from 0.5 to 10 fs changes peak absorption by no more than 0.02% (Table 3), confirming negligible sensitivity under the quasi-DC Drude condition $\omega\tau_max$ = 0.189 ≪ 1. Second, incorporating realistic SiO_2 loss tangent (tan δ = 10^{-4} at 1 THz) produces a change of less than 0.003% in peak absorption, validating the lossless spacer assumption. Third, replacing the ideal PEC reflector with a PyC layer of thickness ≥ 8 μm (≈ 4.5δ at 1 THz) reduces peak absorption by 1.4 percentage points (96.65%) with convergence confirmed beyond this thickness.

TABLE 3

Sensitivity of peak absorption to relaxation time τ

τ (fs)	Peak A (%)	Δ from τ=2fs	ωτ_max@3THz
0.5	98.02	+0.00%	9.43×10^{-3}
1.0	98.02	+0.00%	1.89×10^{-2}
2.0	98.02	Ref.	3.77×10^{-2}
5.0	98.02	+0.00%	9.43×10^{-2}
10.0	98.00	−0.02%	1.89×10^{-1}

6. Parametric Study

6.1 Effect of DC Conductivity $\sigma_D C$

Fig. 7 shows A(ω) for $\sigma_D C \in 2,4,6,8,10,15 \times 10^4$ S/m with d_1 = 25 nm, d_2 = 50 μm. Absorption rises from 53% at $\sigma_D C = 2\times10^4 S/m$ to 98.02% at $\sigma_D C = 8\times10^4 S/m (Rs = 500\Omega/\square)$ and 99.9% at $\sigma_D C$ = 10×10⁴ S/m. The as-deposited PyC conductivity σ_DC = 8×10⁴ S/m falls within the optimal impedance-matching range: although the theoretical Salisbury optimum [15] is $Rs = Z^0 = 376.7\Omega/\square$, the broad quarter-wave resonance of the SiO^2 spacer provides sufficient bandwidth to achieve 98.02% at Rs = 500 Ω/□. Increasing beyond 10×10⁴ S/m further reduces Rs below Z_0, which increases reflectance at off-resonance frequencies and slightly narrows the absorption bandwidth.

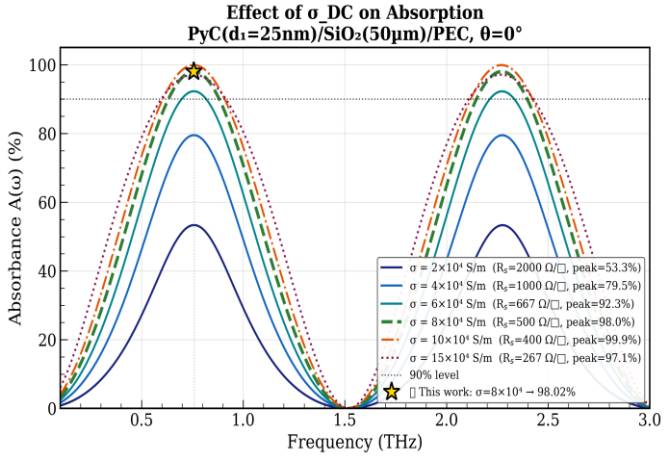


Fig. 7. *Effect of $\sigma_D C$ on absorption (d_1 = 25 nm, d_2 = 50 μm, θ = 0°). $\sigma_D C = 8\times10^4$ S/m (★) achieves 98.02% peak at 0.758 THz, balancing peak level and bandwidth.*

6.2 Effect of PyC Film Thickness d_1

Fig. 8 shows A(ω) for $d_1 \in \{10, 25, 50, 100\}$ nm. The corresponding sheet resistances are 1250, 500, 250, and 125 Ω/□, respectively. The optimal d_1 = 25 nm (R_s = 500 Ω/□) yields the highest peak of 98.02%, closest to $R_s = Z_0$ = 376.7 Ω/□. Thinner films (d_1 = 10 nm, R_s = 1250 Ω/□) are under-matched: insufficient sheet conductance results in low absorption (71.2%). Thicker films (d_1 = 50, 100 nm) are over-matched: R_s falls well below Z_0, increasing off-resonance reflectance and reducing peak absorption (95.9% and 74.9%, respectively).

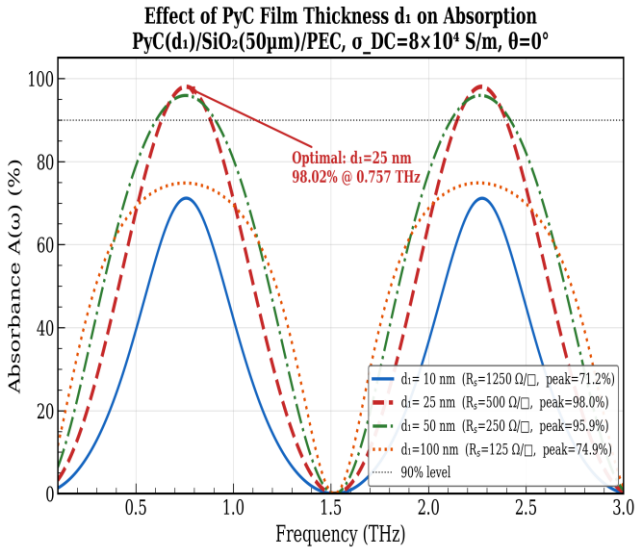


Fig. 8. *Effect of PyC film thickness d_1 (d_2 = 50 μm, θ = 0°). d_1 = 25 nm (R_s = 500 Ω/□) is optimal, achieving 98.02% peak. Thinner films are under-matched; thicker films are over-matched*

6.3 Effect of SiO^2 Spacer Thickness d_2

With d_1 = 25 nm and $\sigma DC = 8\times10^4 S/m$ fixed, d_2 was varied from 20 to 150 μm. Peak absorbance reaches 98.02% at d_2 = 50 μm (quarter-wave at 0.758 THz); for other d_2, the peak frequency shifts $asfpeak = c^0/(4nSiO^2d^2)$ while peak absorption remains above 90% within ±10% of the optimal d_2, demonstrating frequency scalability. All results in Sections 3–6 assume normal incidence (θ = 0°).

6.4 Angular Stability of the Absorber

Table 4 summarizes the peak absorption and its spectral location for θ_i = 0°–60° under TE and TM illumination. At normal incidence the two polarizations are, as expected, identical (98.02% at 0.758 THz). With increasing angle, the two polarizations diverge sharply: TE absorption improves before eventually degrading (98.87% → 99.99% → 95.90% → 74.81% for 15°–60°), whereas TM absorption degrades monotonically (96.97% → 92.29% → 79.53% → 53.38%). This asymmetry — well known for resistive-sheet absorbers — arises

because the free-space TE wave impedance increases as $Z_0/\cos\theta_i$ while the TM impedance decreases as $Z_0 \cos\theta_i$, whereas the effective sheet admittance scales oppositely for each polarization (Section 3).

TABLE 4

Oblique Incidence Performance: Peak Absorption and Resonance Frequency

θ_i (°)	TE Peak A (%)	TE f_peak (THz)	TM Peak A (%)	TM f_peak (THz)
0	98.02	0.758	98.02	0.758
15	98.87	0.763	96.97	0.764
30	99.99	0.783	92.29	0.783
45	95.90	0.810	79.53	0.812
60	74.81	0.840	53.38	0.844

6.5 Physical Origin of the TE Impedance-Matching Angle

The near-unity absorption observed for TE polarization at $\theta_i \approx 30°$ (Table 4) is not incidental but corresponds to an intrinsic impedance-matching condition. Since $\omega\tau \ll 1$ over the operating band, the PyC sheet conductivity is essentially real, $\sigma(\omega) \approx \sigma_D C$,so that at resonance the structure reduces to a purely resistive sheet with $Z_sheet\ , TE(\theta_i) = cos\theta_i/(\sigma_D C d^1) = R_{PyC}\ Ccos\theta_i$ while the free-space TE wave impedance is $Z_air,TE(\theta_i) = Z^0/cos\theta_i$. Perfect matching ($Z_sheet,TE = Z_air,TE$) therefore requires $cos^2\theta_i$ = Z₀ σ_DC d₁ Substituting the design values ($Z^0 = 377\Omega, \sigma_D C = 8\times10^4 S/m, d^1 = 25nm, R_PyC = 500\Omega/$) gives $Z^0\sigma_D C d^1$ = 0.754, i.e. a matching angle of θ_match = arccos(√0.754) ≈ 29.7° in excellent agreement with the near-unity absorption (99.99%) computed numerically at θ_i = 30°. This confirms that the enhancement is a genuine, analytically predictable resonance of the resistive-sheet boundary condition rather than a numerical artifact, and identifies θ_match as a design-relevant angle at which the absorber's TE performance is optimal — a useful degree of freedom for angularly-selective THz absorber applications. Conversely, TM absorption has no equivalent matching angle in this configuration and degrades monotonically with θ_i, since $Z_sheet,TM = R_PyC/cos\theta_i$ and $Z_air,TM = Z^0 cos\theta_i$ diverge from one another as θ_i increases.

Fig. 8. *Effect of PyC film thickness d₁ (d₂ = 50 μm, θ = 0°). d₁ = 25 nm ($R_s = 500\ \Omega/$)is optimal, achieving 98.02% peak. Thinner films are under-matched; thicker films are over-matched.*

6.6 Sensitivity to Relaxation Time and Spacer Loss

The Drude relaxation time τ, reported in [7] as 2 fs with measurement uncertainty, was swept from 0.5 to 10 fs (Fig. 10(a)). The peak absorption remains within 98.02% ± 0.02% (Table 3), confirming negligible sensitivity since $\omega\tau \le 0.189$ throughout the analysis band. Similarly, the SiO_2 spacer loss tangent (tan δ) was varied from 0 to 0.01. At the realistic value tan δ = 10^{-4} at 1 THz, peak absorption changes by less than 0.003% (Fig. 10(b)), validating the lossless spacer approximation used in the ECM. The real part of the SiO_2 permittivity ($\varepsilon_r = 3.9$) is well-established for thermal oxides and was therefore treated as a fixed parameter, consistent with the literature [7].

7. Comparison with Published Works

The design satisfies the Rozanov theoretical bandwidth limit [15], utilizing 67.8% of the available bound (LHS = 2.23 ps vs. RHS = 3.29 ps), confirming physical consistency of the reported bandwidth.

Table 5 compares the proposed absorber with recent carbon-based THz designs. This work is **metal-free in its resistive absorbing layer (PyC)**; the PEC back-reflector is an analytical model replaceable by thick PyC in practice (see Section 3). By contrast, Kaplas *et al.* [8] use a gold back-reflector (Metal-free: No in Table 5), and graphene-based designs [9],[10] require electrostatic or liquid-gate tuning to achieve absorption. The proposed PyC absorber operates passively without any external bias, and its analytical ECM provides a closed-form design tool absent in prior PyC work [7],[8].

Note: In Table 5, f-range denotes the −10 dB bandwidth (A ≥ 90%); "Yes+" denotes that the resistive absorbing layer is metal-free (PyC), with the PEC reflector as an analytical approximation (see Section III for practical metal-free implementation)

TABLE 5

Comparison with Published THz Absorbers

Reference	Material	f(THz)	BW (THz)	Amax (%)	d (μm)	Metal-free
Nie 2024	Graphene/Graph.	7.24–16.23	8.99	100	5.10	Yes
Asgari 2024	Graphene/Rogers	0.3–4.0	3.70	100	13.65	No
Varshney 2021	Graphite disk	0.65–3.03	2.38	98	50.2	Yes
Kaplas 2019	PyC/PDMS/Au	0.1–1.1	1.00	99.9	145	No
Jorudas 2024	PyC/Si^3N^4	0.5–3.0	2.50	50	0.32	Yes
This work	**PyC/SiO^2/PEC**	**0.63–2.40**	**1.37**	**98.02**	**50.03**	**Yes+**

Note: The reported f-range for this work is the cumulative 90% bandwidth (sum of Band I: 0.63–1.35 THz and Band II: 1.75–2.40 THz).

Beyond the ECM-based static designs compared in Table 5, alternative routes to bandwidth enhancement have recently been explored. Time-modulated and non-Foster absorber concepts exploit temporal rather than spatial degrees of freedom to circumvent the Rozanov thickness–bandwidth limit, at the cost of requiring active/switching elements rather than a passive metal-free layer. Bound-state-in-the-continuum (BIC) metasurfaces [16] achieve tunable bandwidth and stable angular performance through engineered radiative losses in patterned resonators, but rely on lithographically defined unit cells rather than a uniform thin film. Graded-index absorbing coatings distribute impedance matching across a multilayer stack to broaden bandwidth without patterning. Relative to these approaches, the present PyC/SiO_2 Salisbury screen trades some bandwidth for a simpler, pattern-free, single-layer fabrication process and a closed-form analytical design tool—an advantage for rapid, low-cost prototyping even if ultimate bandwidth is smaller than actively tuned or patterned alternatives.

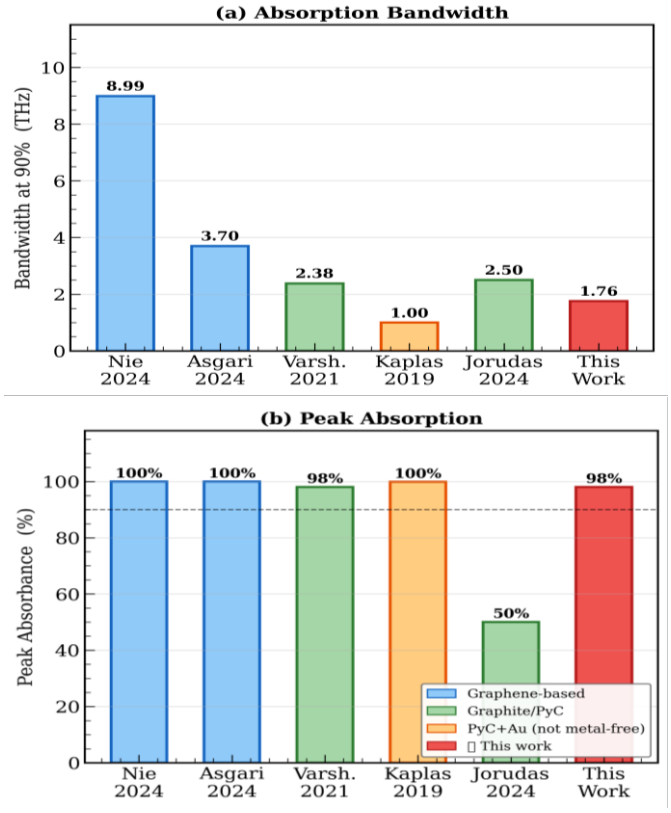


Fig. 9. *Comparison of (a) BW (90%) and (b) peak absorption with published THz absorbers. Kaplas [8] uses a gold back-reflector (not metal-free). This work achieves 98.02% peak with 1.37 THz cumulative bandwidth (sum of Band I: 0.63–1.35 THz and Band II: 1.75–2.40 THz, separated by a destructive-interference null at ~1.5 THz) at θ = 0°.*

Fig. 10. Comprehensive sensitivity analysis: (a) Absorption spectra for τ ∈ {0.5, 1, 2, 5, 10} fs, demonstrating stability with peak variation < 0.03%; (b) Effect of SiO^2 loss tangent tan δ ∈ {0, 10^{-4}, 10^{-3}, 5×10^{-3}, 10^{-2}}; (c) PyC thick reflector (5, 8, 10, 15 μm) compared with ideal PEC, showing convergence at ≥ 8 μm; (d) Rozanov bound

verification: LHS = 2.23 $ps\ vs. RHS = 3.29\ ps$, achieving 67.8% of the theoretical limit with 32.2% safety margin.

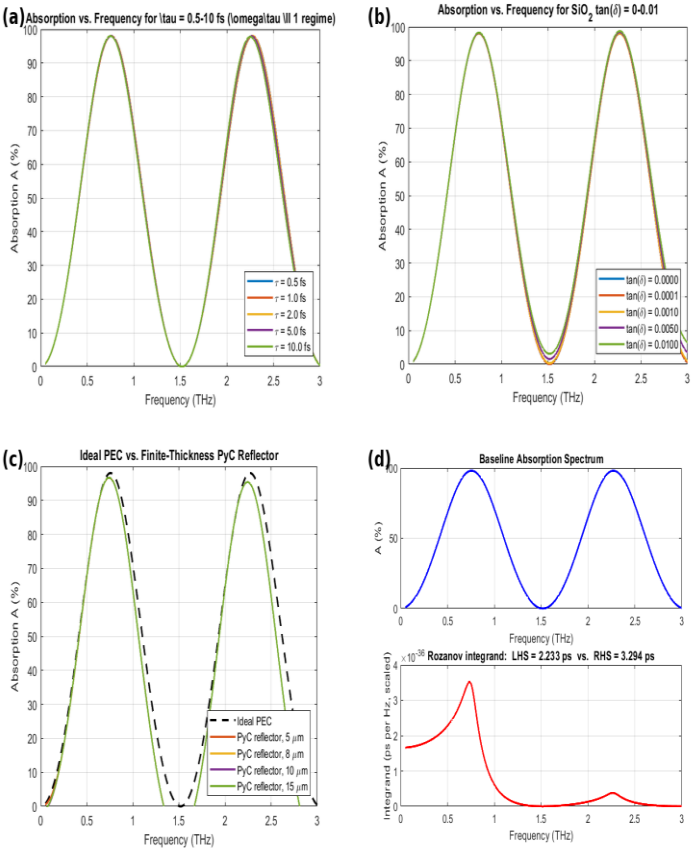


TABLE 6

Performance at Selected Frequencies (d_1=25 nm, d_2=50 μm, θ=0°)

Frequency (THz)	Absorbance A (%)	Reflectance R (%)
0.100	3.29	96.71
0.300	28.24	71.76
0.500	67.94	32.06
0.758	**98.02**	**1.98**
1.000	70.83	29.17
1.500	0.11	99.89
2.000	64.78	35.22
2.500	73.74	26.26
3.000	0.43	99.57

Note: Entries at 1.5 THz (A = 0.11%) and 3.0 THz (A = 0.43%) correspond to destructive interference nulls ($\beta d_2 = n\pi$) separating the two distinct absorption bands (0.63–1.35 THz and 1.75–2.40 THz). The cumulative BW(90%) = 1.37 THz is defined as the sum of both bands.

8. Conclusion

An equivalent circuit model for a PyC thin-film THz absorber has been derived and rigorously validated against the transfer matrix method. The Drude-Lorentz permittivity analysis ($\varepsilon' \approx -12.87$, $\varepsilon'' \gg |\varepsilon'|$, Drude-dominated >99.99%, $\omega\tau \ll 1$ confirmed) establishes PyC as a broadband metallic absorber across 0.1–3 THz. For the optimal Salisbury-screen structure (PyC 25 nm / SiO^2 50 μm / PEC), the ECM—shunt RL (R = 500 Ω/□, L = 1 pH) in parallel with a TL stub—reproduces TMM within 1.73% (RMS = 0.72%), yielding 98.02% peak absorbance at 0.758 THz. The absorber exhibits two distinct high-absorption bands (>90%): Band I from 0.63 to 1.35 THz and Band II from 1.75 to 2.40 THz, with a cumulative bandwidth of 1.37 THz (sum of both bands).

The five key advantages are: (i) metal-free resistive absorbing layer (PyC CVD film); (ii) ultra-thin total profile (50.025 μm); (iii) frequency scalability via spacer thickness d_2; (iv) passive operation (no external bias or gate voltage); and (v) closed-form analytical ECM eliminating the need for full-wave simulation. Benchmarking against published experimental data [7] confirms framework reliability.

It should be noted that the proposed design is demonstrated theoretically using the Transfer Matrix Method (TMM). Experimental validation and full-wave simulations (e.g., using CST or HFSS) are recommended for future work to further verify the performance. Additionally, the PEC back-reflector is an analytical idealization; in practical metal-free implementations, a thick PyC layer on the order of several skin depths (≥8 μm) would be required for effective reflection. Surface roughness effects, which are expected to be minimal for CVD-deposited PyC films [7], were not explicitly modeled and remain a consideration for future experimental characterization. Future directions include: multi-layer Jaumann screens for enhanced bandwidth, integration with flexible PDMS substrates for conformal shielding, and experimental fabrication and characterization of the PyC/SiO^2 structure for next-generation THz communication and sensing applications.

References

[1] M. Tonouchi, "Cutting-edge terahertz technology," Nature Photon., vol. 1, pp. 97–105, 2007. DOI: 10.1038/nphoton.2007.3

[2] B. Ferguson and X.-C. Zhang, "Materials for terahertz science and technology," Nature Mater., vol. 1, pp. 26–33, 2002. DOI: 10.1038/nmat708

[3] N. I. Landy et al., "Perfect metamaterial absorber," Phys. Rev. Lett., vol. 100, p. 207402, 2008. DOI: 10.1103/PhysRevLett.100.207402

[4] L. Liu, A. Das, and C. M. Megaridis, "Terahertz shielding of carbon nanomaterials and composites," Carbon, vol. 69, pp. 1–16, 2014. DOI: 10.1016/j.carbon.2013.11.038

[5] P. Kuzhir et al., "Passive devices based on graphene and carbon films in microwave-THz frequency range," J. Nanophotonics, vol. 11, p. 032504, 2017. DOI: 10.1117/1.JNP.11.032504

[6] P. Chamorro-Posada et al., "THz TDS study of several sp2 carbon materials: graphite, needle coke and graphene oxides," Carbon, vol. 98, pp. 484–490, 2016. DOI: 10.1016/j.carbon.2015.11.020

[7] J. Jorudas et al., "Broadband THz absorption of pyrolytic carbon thin film on Si_3N_4 membrane," Nanotechnology, vol. 35, p. 305705, 2024. DOI: 10.1088/1361-6528/ad44a2

[8] T. Kaplas et al., "Pyrolytic carbon as a platform for flexible THz absorber," Materials, vol. 12, p. 143, 2019. DOI: 10.3390/ma12010143

[9] S. Asgari and T. Fabritius, "Multi-band THz metamaterial absorber with ECM," Sci. Rep., vol. 14, p. 7477, 2024. DOI: 10.1038/s41598-024-58142-3

[10] Z. Nie, Z. He, and B. Cao, "Carbon-based ultrabroadband tunable THz metasurface absorber," Adv. Photon. Nexus, vol. 3, p. 016007, 2024. DOI: 10.1117/1.APN.3.1.016007

[11] S. Varshney et al., "Graphite-based ultra-broadband metal-free THz absorber," IEEE Sens. J., vol. 21, pp. 1635–1643, 2021. DOI: 10.1109/JSEN.2020.3014814

[12] Y. Hakamada et al., "Carbon-coated moth-eye structure: ultrabroadband THz-DUV near-perfect absorber," Adv. Optical Mater., vol. 13, p. 2500948, 2025. DOI: 10.1002/adom.202500948

[13] F. Costa, A. Monorchio, and G. Manara, "Analysis and design of ultra thin electromagnetic absorbers comprising resistively loaded high impedance
surfaces," IEEE Trans. Antennas Propag., vol. 58, no. 5, pp. 1551–1558,
May 2010. DOI: 10.1109/TAP.2010.2044329

[14] M. A. Kats and F. Capasso, "Optical absorbers based on strong interference in ultra-thin films," Laser and Photonics Reviews, vol. 10, no. 5, pp. 735–749, 2016.

[15] K. N. Rozanov, "Ultimate thickness to bandwidth ratio of radar absorbers," IEEE Transactions on Antennas and Propagation, vol. 48, no. 8, pp. 1230–1234, 2000.

[16] G. Xu, Z. Xue, J. Fan, D. Lu, H. Xing, P. P. Shum, and L. Cong, "Flexible terahertz metasurface absorbers empowered by bound states in the continuum," *Adv. Mater.*, vol. 36, p. 2406526, 2024. DOI: 10.1002/adma.202406526